Int. J. Electrochem. Sci., 15 **(2020)** 4138 – 4147, doi: 10.20964/2020.05.15

International Journal of
ELECTROCHEMICAL
SCIENCE
www.electrochemsci.org

Numerical Investigation on the Impact of Membrane Thickness on Transport Phenomena in PEM Fuel Cells

Shian Li[1], *Rongqiang Wei*[1], *Guoling Zhang*[1], *Yuanxin Qi*[2], *Guogang Yang*[1,*], *Qiuwan Shen*[1,*]

[1] Marine Engineering College, Dalian Maritime University, Dalian, China;
[2] Department of Energy Sciences, Lund University, Lund, Sweden;
[*]E-mail: yanggg@dlmu.edu.cn and shenqiuwan@dlmu.edu.cn

Received: 11 December 2019 / *Accepted:* 4 February 2020 / *Published:* 10 April 2020

A two-dimensional mathematical model is used to investigate the performance and transport characteristics of PEM fuel cells with different membrane thicknesses. The overall cell performance of three cases are presented and compared. In addition, the local temperature, liquid water saturation, water content and current density distributions are analyzed and compared. Results show that performance increases with decreasing membrane thickness and the local transport characteristics is also significantly affected. The ohmic loss is mainly caused by the proton transport process inside fuel cell. And a thinner membrane can enhance water back diffusion process in the membrane which is beneficial to the water management at the anode side.

Keywords: PEM fuel cells, Membrane thickness, Cell performance, Transport characteristics

1. INTRODUCTION

Proton exchange membrane (PEM) fuel cells can be used as alternative power sources for various applications [1-7]. PEM fuel cells have not been widely used in practical applications, but the cell performance improvement and cost reduction can promote the commercialization of the PEM fuel cells. Humidified hydrogen and oxygen/air are fed into anode and cathode gas flow channels (GFCs), respectively. The electrochemical reactions take place in catalyst layers (CLs). Water, electricity and heat were simultaneously generated.

Cell performance is determined by the activation loss, ohmic loss and concentration loss. Various flow fields were designed to improve the current density, especially at low cell operating voltages. The non-uniform channels [8-9], wavy channels [10-11], metal foam flow fields [12-13], blocked channels [14-15] and other novel designs [16-17] were extensively investigated and compared to the conventional flow field designs. Generally, cell performance is only improved at the

concentration loss region. This is mainly attributed to the increased mass transfer process. Gas diffusion layers (GDLs) have porous structures made of carbon materials. Usually carbon fiber or carbon cloth is selected as the gas diffusion layer. The thickness of GDL is about 0.2-0.4 mm [18]. And thinner GDL is gradually used in fuel cells to decrease the transfer resistance and then improve the cell performance.

The ohmic loss is mainly caused by the proton transfer through the membrane. The transfer resistance can be decreased with well membrane hydration, while excessive liquid water may result in water flooding issue. The liquid water formation is strongly coupled with temperature distribution. Therefore, water and heat transport processes must be well managed. The water transport process in the membrane is mainly governed by the electro-osmotic drag and back diffusion [19]. The electro-osmotic drag process is from the anode side to the cathode side, while the back diffusion process is from the cathode side to the anode side. The membrane thickness is also gradually decreased to decrease the proton transfer resistance. And the anode side can also be well humidified due to the increased back diffusion process. A two-dimensional fuel cell model was developed and used to study the impact of membrane thickness on transport processes and cell performance. The temperature, liquid water saturation and water content distributions in fuel cells with different membrane thickness were presented and analyzed. In addition, the polarization curve and power density curve were compared.

2. MATHEMATICAL MODEL DESCRIPTION

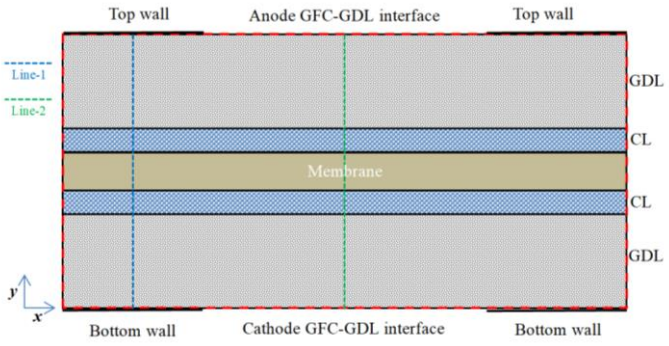

Figure 1. Schematic of the computational domain.

Table 1. Geometric parameters and operating conditions.

Parameter	Value	Unit
Cell width	2	mm
GFC width	1	mm
Anode/Cathode GDL thickness	0.2	mm
Anode/Cathode CL thickness	0.01	mm
Operating pressure	1.0	atm
Operating temperature	353	K

The physical model used in this study is shown in Figure 1. Line-1 represents the middle position of walls, and Line-2 denotes the middle position of cell. The thickness of GDL is 0.2mm, and the thickness of CL is 0.01mm. Three different membranes (Nafion N117, NR211 and NR212) are used in this study. As shown in Table 1, the detailed geometric parameters and the operating conditions are summarized. The following assumptions are used in this mathematical model: laminar flow; ideal gas; homogeneous and isotropic CLs; generated water in dissolved phase [20].

2.1 Governing equations

The governing equations are summarized in Table 2, and the corresponding source terms are shown in Table 3. And the corresponding expressions and parameters refer to our previous study [20].

Table 2. Governing equations

Descriptions	
Species conservation equation:	$0 = \nabla \cdot \left(\rho D_{eff,i} \nabla Y_i\right) + S_i$
Energy conservation equation:	$0 = \nabla \cdot \left(k_{eff} \nabla \mathrm{T}\right) + S_T$
Charge conservation equation:	$\nabla \cdot \left(\sigma_{eff,s} \nabla \phi_s\right) + S_s = 0$ $\nabla \cdot \left(\sigma_{eff,m} \nabla \phi_m\right) + S_m = 0$
Liquid water transport equation:	$0 = \nabla \cdot (\rho_l D_s \nabla s) + S_l$
Dissolved water transport equation:	$-\nabla \cdot \left(\frac{n_d}{F} \sigma_m \nabla \phi_m\right) = \nabla \cdot \left(\frac{\rho_m}{M_m} D_\lambda \nabla \lambda\right) + S_d$

2.2 Boundary conditions

The fuel cell model is modeled in ANSYS FLUENT by using the user defined functions. Hydrogen and water vapor mass fractions are prescribed at the anode GFC-GDL interface, and the oxygen and water vapor mass fractions are specified at the cathode GFC-GDL interface. The water saturation level is set as zero at the above mentioned interfaces. Operating temperature is applied at the top and bottom walls. In addition, $\phi_s=0$ and $\phi_s=V_{cell}$ are defined at the top and bottom walls.

Table 3. Source terms of the corresponding governing equations.

Descriptions	Units
$S_{H_2} = -\frac{j_a}{2F} M_{H_2} \quad Anode\ CL$	kg m^{-3} s^{-1}
$S_{O_2} = -\frac{j_c}{4F} M_{O_2} \quad Cathode\ CL$	kg m^{-3} s^{-1}

$S_{wv} = -S_l - S_{vd}M_{H_2O}$ $Anode\ and\ cathode\ CLs$	kg m^{-3} s^{-1}
$S_{wv} = -S_l$ $Anode\ and\ cathode\ GDLs$	
$S_T = j_a\eta_a - \frac{T\Delta S_a}{2F}j_a + \sigma_{eff,m}\|\nabla\phi_m\|^2 + \sigma_{eff,s}\|\nabla\phi_s\|^2 + (S_l - S_{ld})\Delta h_{lg}$ $Anode\ CL$	W m^{-3}
$S_T = j_c\eta_c - \frac{T\Delta S_c}{4F}j_c + \sigma_{eff,m}\|\nabla\phi_m\|^2 + \sigma_{eff,s}\|\nabla\phi_s\|^2 + (S_l - S_{ld})\Delta h_{lg}$ $Cathode\ CL$	
$S_T = \sigma_{eff,m}\|\nabla\phi_m\|^2$ $membrane$	
$S_T = \sigma_{eff,s}\|\nabla\phi_s\|^2 + S_l\Delta h_{lg}$ $Anode\ and\ cathode\ GDLs$	
$S_s = -j_a$ $Anode\ CL$	A m^{-3}
$S_s = +j_c$ $Cathode\ CL$	
$S_m = +j_a$ $Anode\ CL$	A m^{-3}
$S_m = -j_c$ $Cathode\ CL$	
$S_l = S_{phase} - S_{ld}$ $Anode\ and\ cathode\ GDLs\ and\ CLs$	kg m^{-3} s^{-1}
$S_{phase} = \begin{cases} \gamma_{cond}\frac{\varepsilon(1-s)}{RT}M_{H_2O}(P_{wv} - P_{sat}) & P_{wv} \geq P_{sat} \\ \gamma_{evap}\frac{\varepsilon s}{RT}M_{H_2O}(P_{wv} - P_{sat}) & P_{wv} < P_{sat} \end{cases}$	kg m^{-3} s^{-1}
$S_d = S_{vd} + S_{ld}$ $Anode\ CL$	mol m^{-3} s^{-1}
$S_d = S_{vd} + S_{ld} + S_\lambda$ $Cathode\ CL$	
$S_{vd} = (1-s)\gamma\frac{\rho_m}{M_m}(\lambda^{eq} - \lambda)$ $Anode\ and\ cathode\ CLs$	
$S_{ld} = s\gamma\frac{\rho_m}{M_m}(\lambda^{eq} - \lambda)$ $Anode\ and\ cathode\ CLs$	
$S_\lambda = \frac{j_c}{2F}$ $Cathode\ CL$	

3. RESULTS AND DISCUSSION

As shown in Fig.2, cell performance of three cases is given and compared. Case A is the thickest one, and case C is the thinner one. Cell performance is evaluated in terms of polarization curve. And the corresponding power density curves are also presented. It is clear that the current density is greatly increased with decreasing membrane thickness. The ohmic loss is mainly caused by the transport process of proton. And the transport resistance is decreased, when the thickness is decreased and the proton conductivity is kept constant [21]. The current densities of three cases are 0.972 A/cm^2, 1.258 A/cm^2 and 1.366 A/cm^2 at the cell voltage 0.3 V, respectively. And the corresponding power densities of three cases are 0.291 W/cm^2, 0.377 W/cm^2 and 0.410 W/cm^2, respectively.

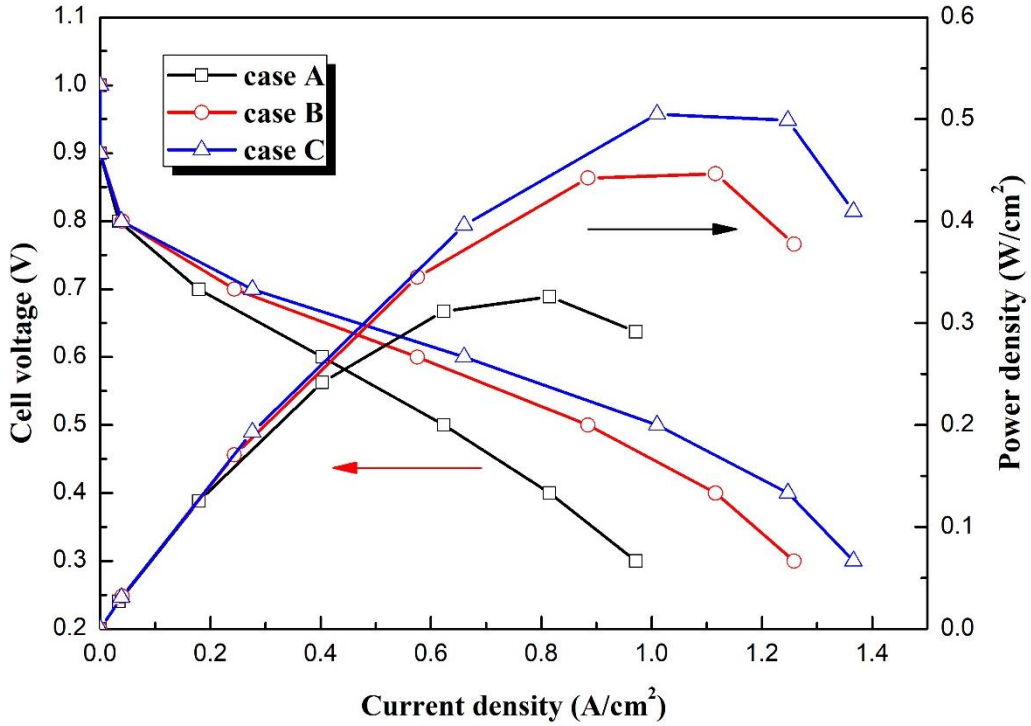

Figure 2. Cell performance of three cases.

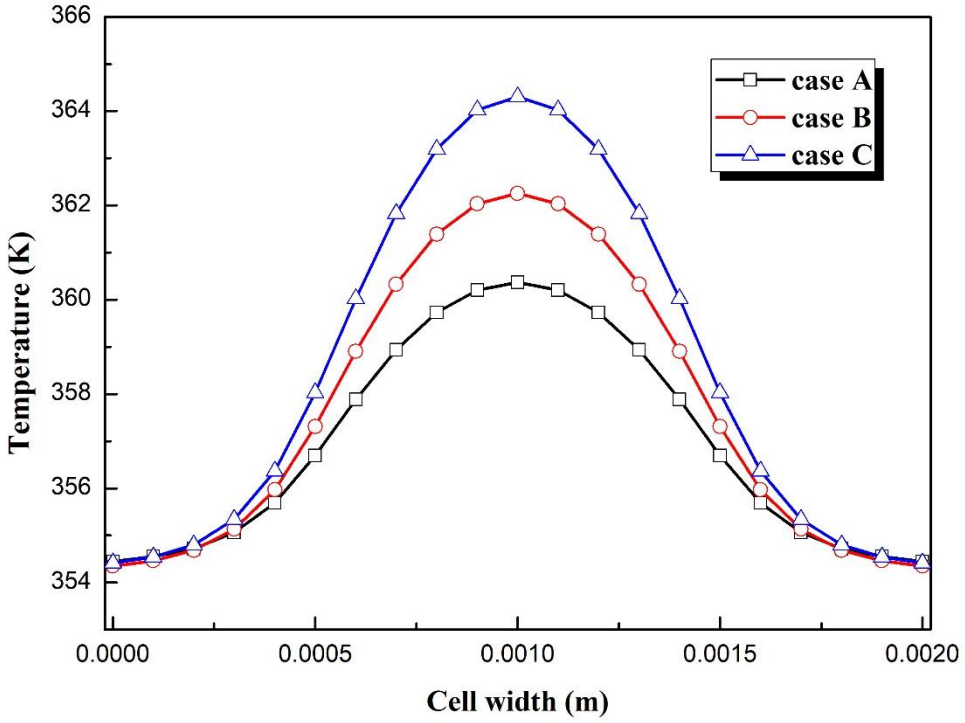

Figure 3. Temperature distributions of three cases at the cell voltage 0.3 V.

The temperature distributions of three cases at the cathode GDL-CL interface are presented in Fig.3. It is clearly seen that the maximum temperature is at the middle region of the cell, and the

minimum temperature is at the lateral region of the cell. The generated heat inside fuel cells is transferred through the lateral regions to the current collectors and the temperature of current collector is kept constant due to the existence of cooling channels [22]. The minimum temperatures of three cases are almost the same, while the maximum temperatures of three cases are different. The maximum temperatures of three cases are 360.36 K, 362.25 K and 364.30 K, respectively.

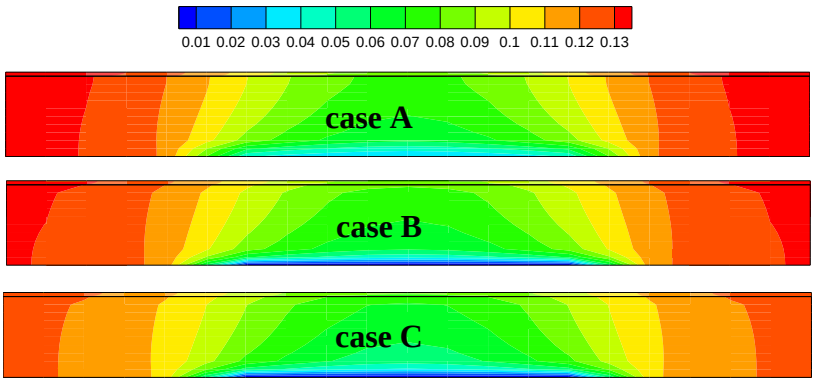

Figure 4. Liquid water saturation distributions at the cathode GDL and CL of three cases at the cell voltage 0.3 V.

The liquid water saturation distributions at the cathode GDL and CL of three cases are shown in Fig.4. In addition, the liquid water distributions of three cases at the cathode GDL-CL interface are presented in Fig.5. It is clearly seen that liquid water saturation level at the lateral regions is greater than that at the middle region of cells. This is because of the temperature distributions as mentioned above.

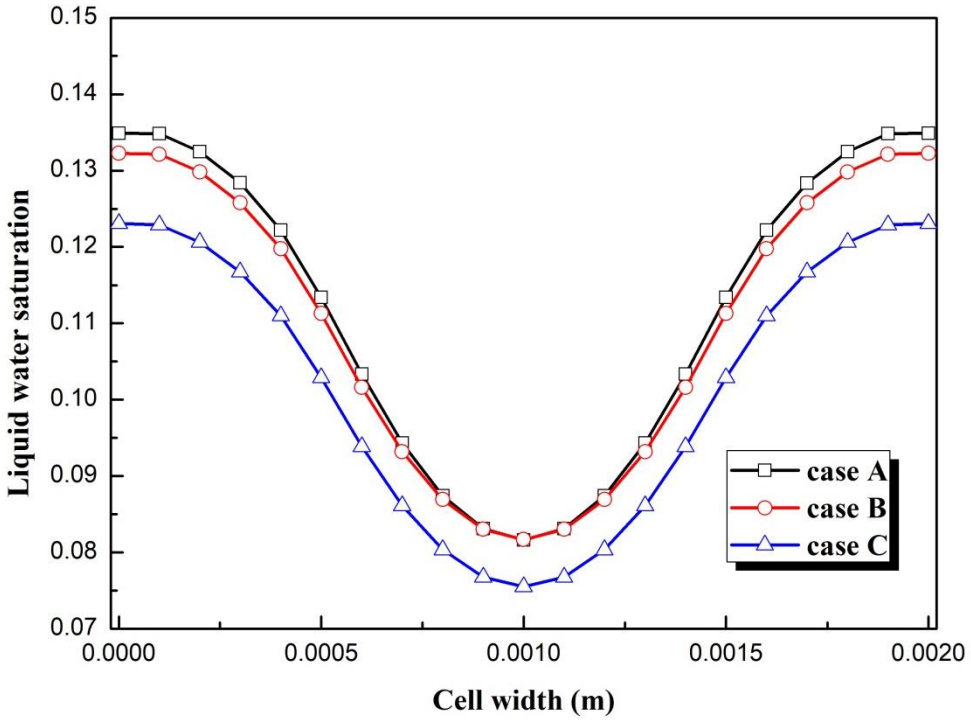

Figure 5. Liquid water saturation distributions of three cases at the cell voltage 0.3 V.

The maximum and minimum liquid water saturation levels of case A are 0.135 and 0.082, respectively. The maximum and minimum liquid water saturation levels of case B are 0.132 and 0.082, respectively. The maximum and minimum liquid water saturation levels of case C are 0.123 and 0.075, respectively. The liquid water saturation level decreases due to the increase in temperature. The liquid water formation and transportation is strongly coupled with the heat, mass and charge transport processes inside fuel cells [23].

The water content in the membrane at the Line-1 and Line-2 of three cases are shown in Figs.6-7. It can been seen that the water content is decreased from the cathode side to the anode side and the water content at the lateral region is greater than that at the middle region of cells. For case A, the water content is decreased from 15.07 to 4.98 at Line-1. For case B, the water content is decreased from 14.39 to 5.97 at Line-1. For case C, the water content is decreased from 12.95 to 7.32 at Line-1. Similarly, the water content of case A is decreased from 12.39 to 4.33 at Line-2. The water content of case B is decreased from 11.71 to 4.79 at Line-2. The water content of case C is decreased from 10.22 to 5.63 at Line-2. This indicates that the water content variation through the membrane decreases when the membrane thickness decreases. The water transport processes is determined by the electro-osmotic drag and back diffusion. The electro-osmotic drag process is related to the current density, and the back diffusion process is related to the concentration of water [19]. The membrane with thinner thickness facilitates the back diffusion from cathode side to anode side. In addition, the water transport processes are affected by the absorption and desorption processes in the anode and cathode CLs [24].

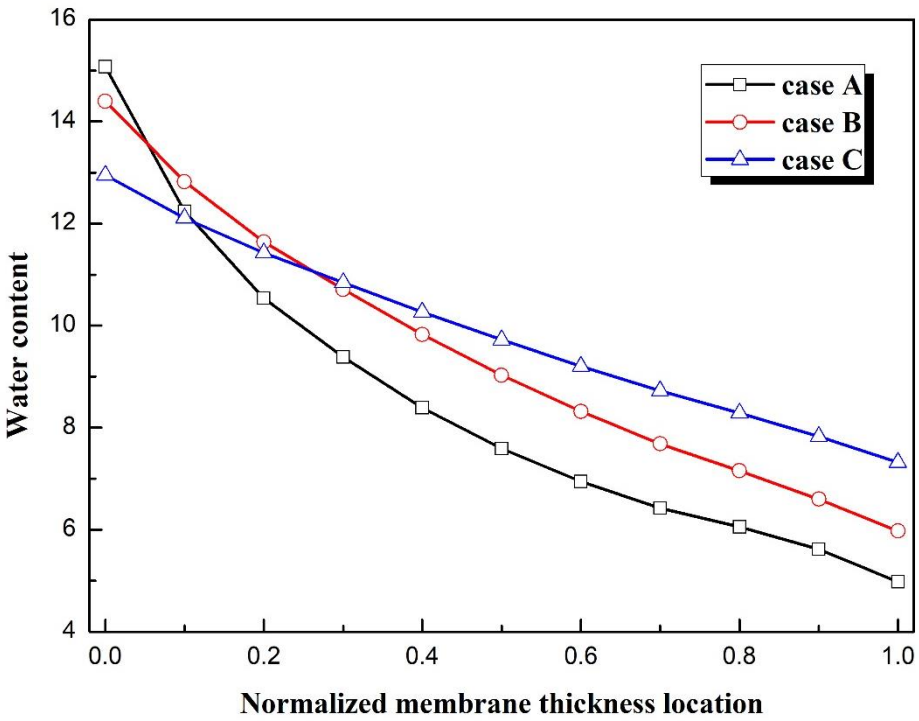

Figure 6. Water content distributions of three cases (Line-1) at the cell voltage 0.3 V.

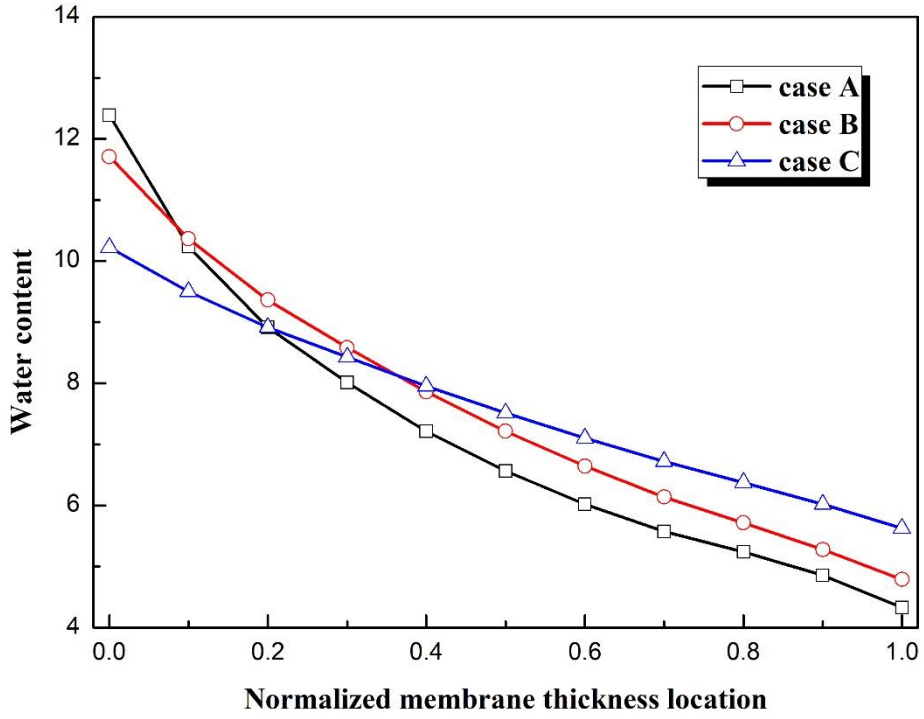

Figure 7. Water content distributions of three cases (Line-2) at the cell voltage 0.3 V.

.

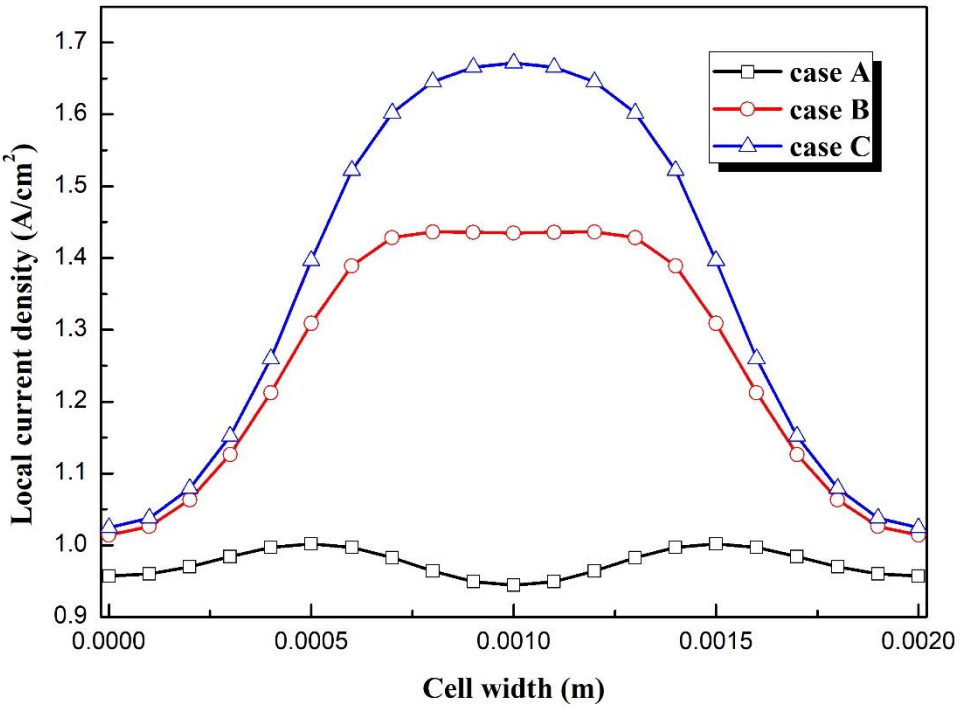

Figure 8. Local current density distributions of three cases at the cell voltage 0.3 V.

The local current densities of three cases are shown in Fig.8. As expected, the maximum local current density is provided by case C followed by case B and case A. The profiles of three cases are also different. The maximum current densities of case B and case C are at the middle of cells, while the

minimum current density is at the lateral of cells. For case A, the maximum current densities are at the x=0.0005 m and x=0.0015 m position and the minimum current density is at the cell middle region. It is concluded that the local current density distribution of fuel cell is also strongly affect by the membrane thickness.

4. CONCLUSIONS

The performance and transport characteristics of PEM fuel cells with different membrane thicknesses are numerically investigated. The current density is greatly increased with decreasing membrane thickness, when the operating voltage is kept constant. The local temperature is increased with decreasing membrane thickness, while the liquid water saturation is decreases with decreasing membrane thickness. Water content variation through the membrane is decreased with decreasing membrane thickness due to the back diffusion effect. In addition, the local current density distribution is also strongly affected by the membrane thickness. With the development of technology, the membrane thickness is gradually decreased. This study can provide detailed information on the performance and transport characteristics of PEM fuel cells with different membrane thicknesses.

ACKNOWLEDGEMENTS
This work is funded by the National Natural Science Foundation of China (No.51779025), the Fundamental Research Funds for the Central Universities of China (No.3132019327), China Postdoctoral Science Foundation (No.2019M651097 and No.2019M651094) and Natural Science Foundation of Liaoning Province (No.2019-BS-026 and No.2019-ZD-0154).

References

1. Y. Wang, K.S. Chen, J. Mishler, S.C. Cho, X.C. Adroher, *Appl. Energy,* 88 (2011) 981.
2. T.D. Tran, S. Huang, D.H. Vu, V.N. Duy, *Int. J. Electrochem. Sci.,* 13 (2018) 10480.
3. S.A. Li, R.Q. Wei, Y.X. Qi, G.G. Yang, Q.W. Shen, *Int. J. Electrochem. Sci.,* 14 (2019) 11367.
4. B. Lee, K. Park, H.M. Kim, *Int. J. Electrochem. Sci.,* 8 (2013) 219.
5. S.A. Li, B. Sunden, *Int. J. Hydrogen Energy* 43 (2018) 16279.
6. S.A. Li, J.L. Yuan, G.N. Xie, B. Sunden, *Numer. Heat Transfer A,* 72 (2017) 807.
7. S.A. Li, J.L. Yuan, M. Andersson, G.N. Xie, B. Sunden, *Int. J. Energy Res.*, 41 (2017) 2034.
8. E. Fontana, E. Mancusi, A. Silva, V.C. Mariani, A.A.U. Souza, S.M.A.G.U. Souza, *Int. J. Heat Mass Transfer*, 54 (2011) 4462.
9. H.C. Liu, W.M. Yan, C.Y. Soong, F. Chen,H.S. Chu, *J. Power Sources*, 158 (2006) 78.
10. J.K. Kuo, T.H. Yen, C.K.Chen, *J. Power Sources*, 177 (2008) 96.
11. S.A. Li, J.L. Yuan, M. Andersson, G.N. Xie, B. Sunden, *J. Electrochem. Energy Convers. Storage*, 14 (2017) 031007.
12. S.A. Li, B, Sunden, *Int. J. Hydrogen Energy,* 42 (2017) 27323.
13. C.J. Tseng, B.T. Tsai, Z.S. Liu, T.C. Cheng, W.C. Chang, S.K. Lo, *Energy Convers. Manag.,* 62 (2012) 14.
14. S.W. Perng, H.W. Wu, *Appl. Energy,* 88 (2011) 52.

15. A. Azarafza, M.S. Ismail, M. Rezakakazemi, M. Pourkashanian, *Renew. Sust. Energ. Rev.,* 116 (2019) 109420.
16. H.C. Kang, K.M. Jum, Y.J. Sohn, *Int. J. Hydrogen Energy,* 44 (2019) 24036.
17. M. Whiteley, J.I.S. Cho, L. Rasha, T. Neville, J. Millichamp, R. Luca, P.R. Shearing, D.J.L. Brett, *J. Power Sources*, 442 (2019) 227218.
18. L. Cindrella, A.M. Kannan, J.F. Lin, K. Saminathan, Y. Ho, C.W. Lin, J. Wertz, *J. Power Sources*, 194 (2009) 146.
19. T.E. Springer, T.A. Zawodzinski, S. Gottesfeld, *J. Electrochem. Soc.*, 138 (1991) 2334.
20. S.A. Li, J.L. Yuan, G.N. Xie, B. Sunden, *Int. J. Hydrogen Energy,* 43 (2018) 8451.
21. T.E. Springer, M.S. Wilson, S. Gottesfeld, *J. Electrochem. Soc.*, 140 (1992) 3513.
22. S.A. Li, B. Sunden, *Numer. Heat Transfer A,* 74 (2018) 917.
23. Y. Wang, C.Y. Wang, *J. Electrochem. Soc.,* 153 (2006) A1193.
24. H. Wu, X.G. Li, P. Berg, *Electrochim. Acta*, 54 (2009) 6913.